JOWRM

Journal of Water Resources Management

Journal homepage: https://journal.water.gov.my

e-ISSN: 2811-3578

Harnessing Wave Energy through Hinged-Type WEC Integrated with Existing Jetty Infrastructure: A Case Study of Bintulu, Malaysia

Hooi-Bein Goh[1*]

1 Global Water Consultants Sdn. Bhd.

**Corresponding Author; jasminegoh.gwc@gmail.my*

Email: jasminegoh.gwc@gmail.my

Received 15 June 2026;
Accepted 16 Oct 2026;
Available online 21 Oct 2026

Abstract: This study assesses the feasibility of deploying hinged-flap Wave Energy Converters (WECs) along a 3 km section of the Bintulu jetty, Sarawak, Malaysia, using a coupled Delft3D-HD and SWAN modelling framework. High-resolution hydrodynamic and wave simulations, validated against Acoustic Doppler Current Profiler (ADCP) data, captured site-specific monsoonal variability. Results indicate that the Northeast Monsoon provides the most favourable operating conditions, with significant wave heights of 1.0–1.2 m and peak periods of 7–8 s, corresponding to wave energy fluxes of 3.4–5.6 kW/m. Accounting for realistic engineering parameters—capture width ratio, power take-off efficiency, availability, and array interaction losses—the projected annual energy production ranges from 161–269 MWh/year (conservative) to 844–1,406 MWh/year (optimistic), equivalent to powering 40–67 and 211–352 households respectively. The integration of hinged-flap WECs into existing maritime infrastructure offers a cost-effective and spatially efficient approach for renewable energy generation in monsoon-dominated coastal zones. These findings support further investigation into long-term resource variability, techno-economic optimisation, and pilot-scale deployment.

Keywords: Wave energy converter; Delft3D-SWAN modelling; Hydrodynamic calibration; Monsoon wave climate; Coastal renewable energy

1. Introduction

In Malaysia, wave conditions are largely governed by the Northeast (NE) and Southwest (SW) monsoons, which influence seasonal wave energy availability (Mazlan et al., 2020; Zhang, Li & Lin, 2022). Among various WEC technologies, the bottom-hinged oscillating flap type is well suited for deployment in shallow water environments, exhibiting efficient energy capture in moderate sea states (Falnes, 2007; Folley, Whittaker & Henry, 2007; Whittaker & Folley, 2012).

This study aims to evaluate the feasibility of deploying hinged-type WECs along the Bintulu coastal jetty. A numerical modelling framework using Delft3D-FLOW coupled with SWAN was employed to simulate site-specific hydrodynamics and wave climate. Calibration and validation were performed using field data from Acoustic Doppler Current Profilers (ADCPs). The resulting wave energy flux and annual energy output were analysed to assess the suitability of this technology under local wave conditions.

2. Methodology

This study employs a numerical modelling approach to assess the wave energy potential and hydrodynamic conditions at the Bintulu jetty site. The Delft3D modelling suite, specifically the Hydrodynamic (HD) and Wave modules, is used to simulate tidal currents, water levels, and wave climate in the region.

2.1 Study Area

The study area is situated offshore of Bintulu, Sarawak, in the South China Sea (Figure 1), where a 3 km pile-supported jetty (Figure 1) is proposed for wave energy conversion using hinged-flap type wave energy converters (WECs). The region features a shallow continental shelf with water depths ranging from 5 to 20 m, displaying a gently sloping seabed with minor undulations and localized sand wave formations (Abdullah et al., 2022). Sediment analysis reveals a dominant composition of fine to medium sand, with intermittent silty clay deposits in deeper zones, indicative of mixed fluvial-marine sedimentation processes (Tan et al., 2021).

**Corresponding author: jasminegoh.gwc@gmail.my*
2026 JPS Publishing. All right reserved.

The area experiences mixed, predominantly diurnal tides (mean range: 2–3 m) and is influenced by strong monsoonal winds, with significant wave heights reaching 1.5–3.5 m during the northeast monsoon (Mazlan et al., 2020). The sandy seabed provides moderate to high bearing capacity, though localized soft clay layers necessitate geotechnical adaptation for pile-supported structures (Yusof et al., 2019). Integrating WECs with existing maritime infrastructure offers a cost-effective pathway for marine renewable energy deployment in Malaysia and similar tropical coastal regions (Omar & Samad, 2023).

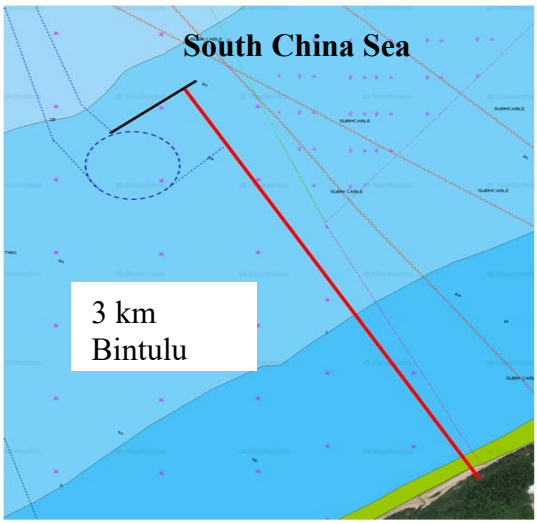

Fig.1-Layout of the 3 km Bintulu Jetty

2.2 Data Collection

To characterise local hydrodynamics, two Acoustic Doppler Current Profilers (ADCPs) were deployed at nearshore locations with coordinates and depths as summarised in Table 1 and Figure 2. Water level and current velocity data were collected continuously over 17 days between 15th and 30th June 2024, covering both spring and neap tide conditions. The ADCPs recorded data at 10-minute intervals with vertical resolution of 0.5 m. The measurements were used for calibrating the Delft3D-FLOW hydrodynamic model.

Table 1. ADCP Deployment Information

Station	Longitude	Latitude	Seabed Level (mMSL)
ADCP 1	113° 5′40.52″E	3°19′9.80″N	5.5
ADCP 2	113° 5′2.97″E	3°18′33.86″N	4.7



Fig.2-Locations of ADCPs

Hindcasted metocean data, including wind and wave parameters, were obtained from the Global Reanalysis of Ocean Wave 2012 (GROW) dataset for the offshore region of the project site, located at 4°0′0.00″ N, 113°0′0.00″ E as shown in Figure 3. The GROW dataset provides global coverage with a spatial resolution of 0.5° and an hourly time series of wave and wind parameters over a 9-year period from 2003 to 2012 (GROW, 2012).

This dataset was used to define offshore boundary conditions for the wave model and to characterize the regional wave climate. Parameters such as significant wave height (H_s), peak wave period (T_p), and mean wave direction (T_m), along with wind speed and direction, were extracted approximately 81.7 km offshore from Tanjung Kidurong in the South China Sea. These data supported the calibration and validation of wave transformation processes within the coupled Delft3D-SWAN modelling framework.

The use of long-term hindcast data ensures that the model captures a representative range of wave conditions, including extreme and seasonal events, essential for reliable wave energy assessment and design load estimation.

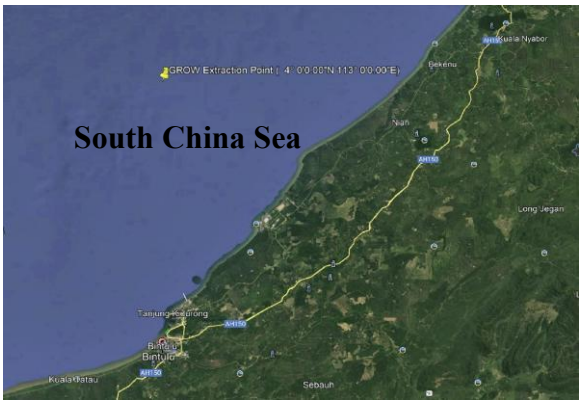

Fig. 3- Location of GROW data extraction point

To characterise local hydrodynamics, two Acoustic Doppler Current Profilers (ADCPs)

2.3 Numerical Model Setup

Figure 4 illustrates the model domain and grid resolution, highlighting the high-resolution mesh around the jetty structure.

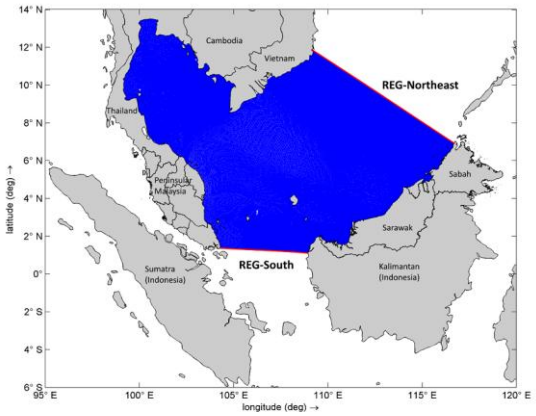

Fig. 4 - Model domain and grid resolution map

The Wave module within Delft3D is coupled dynamically with the HD module, enabling two-way feedback between wave action and hydrodynamics. The wave model resolves wave propagation, refraction, shoaling, and breaking, considering local bathymetry and coastal features (Deltares, 2023).

These outputs are integrated into a performance model for hinged-type wave energy converters (WECs) deployed along or near the jetty. The hinged-type WEC operates by converting the pitching motion induced by passing waves into mechanical energy. The device typically consists of multiple buoyant segments connected by hinges that allow rotation relative to one another. The relative motion across these hinges is resisted by hydraulic or mechanical systems that generate power (Folley, Whittaker & Henry, 2007; Pecher & Kofoed, 2017).

At this feasibility stage, the hinged-flap WEC was represented using a frequency-domain response-function approach rather than a fully coupled CFD-structural solver. The SWAN-derived wave spectra at the jetty were used as the incident energy input, while the device response was represented using benchmark bottom-hinged flap/Oyster-type response concepts from Falnes (2007), Folley et al. (2007), Whittaker and Folley (2012), and Pecher and Kofoed (2017).
For each wave frequency, the absorbed power is estimated by multiplying the frequency-dependent device response function, $R(\omega)$, by the local wave spectral energy density, $S(\omega)$, and integrating over the frequency domain. This formulation provides a transparent feasibility-level estimate of extractable power before applying practical conversion factors such as capture width ratio, PTO efficiency, availability and array interaction losses.
The approach is suitable for screening deployment potential and comparing seasonal energy yield, but the results should be refined using device-specific power matrices, prototype testing and detailed structural-hydrodynamic coupling during subsequent design stages.

This modelling approach supports assessment of spatial and temporal variability of wave energy availability, identification of optimal device placement, and techno-economic viability of hinged-type WEC deployment at the Bintulu jetty.

2.4 Model Domain and Boundary Conditions

Hydrodynamic boundary conditions are imposed at the open ocean boundaries of the model domain. A regional hydrodynamic model of the South China Sea was developed using the Delft Dashboard (DDB) tool to simulate complex flow patterns driven by tidal and wind-induced circulation (Deltares, 2023). The model domain covers a broad area with a grid resolution of approximately 2.8 km × 4.0 km. Bathymetric input was sourced primarily from the General Bathymetric Chart of the Oceans (GEBCO), providing sufficient detail for resolving regional-scale topographic features (Weatherall et al., 2015). A large domain was essential to accurately represent basin-wide dynamics and interactions influencing the coastal zone. The spatial grid coverage and bathymetric setup for the regional model is shown in Figure 5.

Tidal forcing along the open boundaries was specified using tidal harmonic constituents from the TPXO7.2 Global Model of Ocean Tides (Egbert and Erofeeva, 2002). The model included eight primary constituents (M2, S2, N2, K2, K1, O1, P1, Q1), two long-period constituents (Mf and Mm), and three shallow water non-linear constituents (M4, MS4, MN4), all applied at a global resolution of 0.25°. Two main open boundaries—REG-Northeast and REG-South—were imposed within the regional model. Water level boundary conditions were assigned using tidal series from nearby ports located closest to the boundary nodes, serving as the dominant external forcing mechanism for the model.

A nested modelling approach was adopted to optimize computational efficiency while maintaining high-resolution accuracy in the nearshore region. This technique allows a high-resolution local model to retrieve boundary conditions from a larger-scale coarser regional model, thereby reducing computational demand without compromising hydrodynamic detail (Deltares, 2023).

A curvilinear structured grid was developed for the local model, covering approximately 54.06 km along the Bintulu coastline, with maximum seaward extent reaching up to 14.11 km offshore. The grid resolution varies from coarse cells of 286 m × 278 m in the outer seaward area to fine-scale resolution of 20 m × 16 m near the proposed project location (Figure 6a), enabling accurate simulation of tidal and wave interactions in shallow and structurally complex areas. The bathymetry used to construct the local model grid was compiled from multiple sources, including site-specific bathymetric survey data, digitized Admiralty charts, and in-house datasets (Figure 6b). These data were interpolated and quality-checked to ensure topographic continuity and consistency across the computational mesh. The bottom roughness was represented with a roughness value of 0.02 $s/m^{1/3}$ (Deltares, 2023).

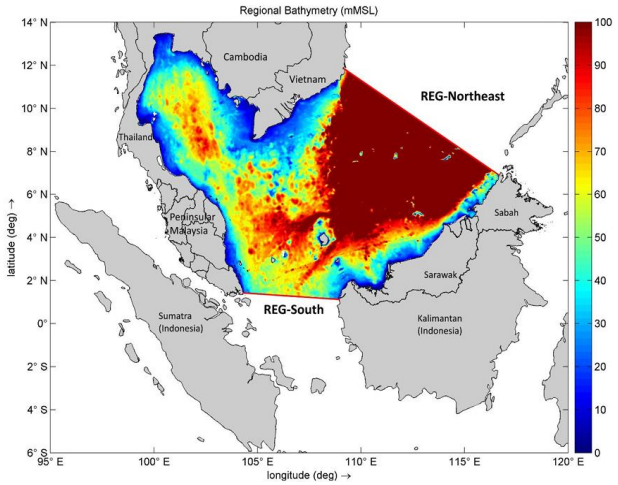

Fig.5-Regional model bathymetry within the boundary conditions (REG-South, REG-Northeast)

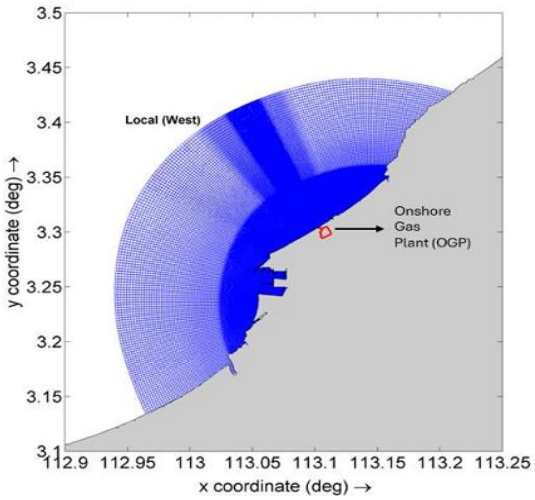

Figure 6a. Local Model Grid

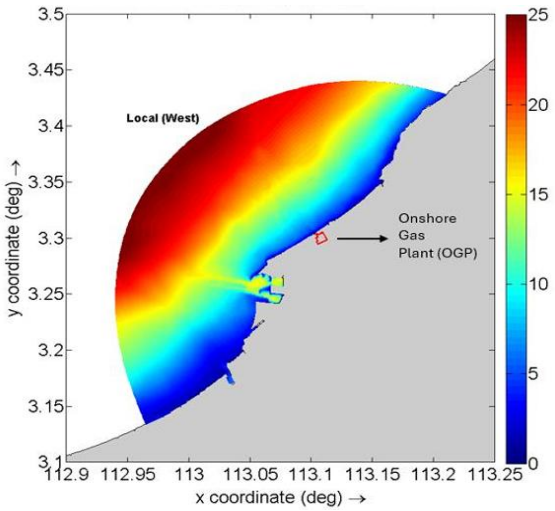

Fig.6b-Local Model Bathymetry

Table 2. Summary of the key model parameters, boundary conditions, and forcing data sources.

Component	Parameter / Description	Source / Reference
Model Domain	South China Sea regional grid, ~2.8 km × 4.0 km resolution	This study
Bathymetry	GEBCO global bathymetric dataset	Weatherall et al. (2015)
Hydrodynamic Model	Delft3D-HD v4.03	Deltares (2023)
Wave Model	SWAN v41.31 coupled with Delft3D	Delft3D/SWAN framework
Tidal Forcing	8 primary constituents (M2, S2, N2, K2, K1, O1, P1, Q1); 2 long-period (Mf, Mm); 3 nonlinear (M4, MS4, MN4)	TPXO7.2 (Egbert and Erofeeva, 2002)
Open Boundaries	REG-Northeast and REG-South	This study
Water Level Forcing	Tidal series from nearby tide gauge stations	Local ports / field data
Wind Forcing	Wind speed and direction for wave generation and transformation	GROW
Grid Type	Curvilinear structured grid; finer nearshore (~10–20 m), coarser offshore	This study

2.5 Model Calibration and Validation

Two Acoustic Doppler Current Profilers (ADCPs) were deployed near the jetty to collect high-resolution measurements of tidal currents and water levels over a representative period covering spring and neap tides. These observations enable calibration of the hydrodynamic model parameters, including bottom roughness and friction coefficients, ensuring accurate reproduction of tidal amplitude and current velocity.

Model performance was evaluated quantitatively by comparing simulated and observed data using RMSE together with Nash-Sutcliffe Efficiency (NSE) as a complementary model-skill indicator. RMSE measures absolute error, while NSE provides additional information on temporal variability, correlation and bias (Moriasi et al., 2007).

$$RMSE = \sqrt{\frac{1}{N}\sum_{i=1}^{N}(S_i - O_i)^2}$$

where Si is the simulated value, Oi is the observed value and N is the number of paired observations.

In response to the reviewer recommendation, NSE was adopted as the additional reported performance measure for the ADCP calibration and validation.

$$NSE = 1 - [\frac{\Sigma(S_i - O_i)^2}{\Sigma(S_i - O_{mean})^2}]$$

where S_i is the simulated value, O_i is the observed value, O_{mean} is the mean observed value. Values closer to 1 indicate stronger model performance.

2.6 SWAN Model Coupling

The Simulating Waves Nearshore (SWAN) model (version 41.31) is coupled with Delft3D-HD to enhance wave modelling fidelity. SWAN's spectral wave model captures detailed wave dynamics influenced by local bathymetry, wind, and current interactions, especially in shallow coastal areas where wave transformation is complex. The coupled system allows iterative exchange of wave and hydrodynamic parameters at defined time steps to reflect their mutual feedback.

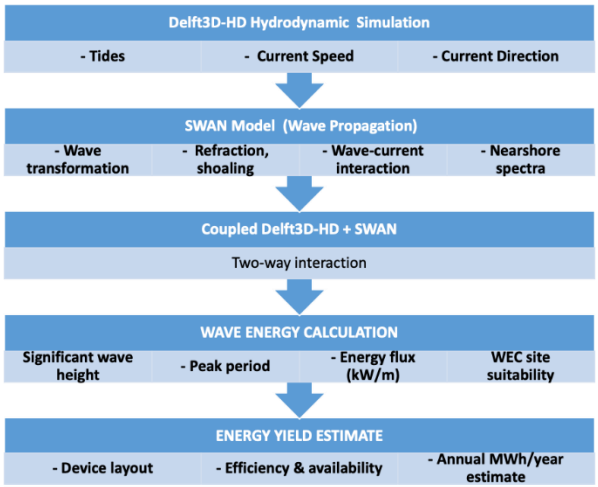

Fig.7-Flowchart of the coupled Delft3D-HD and SWAN modelling framework.

2.7 Wave Energy Potential Assessment

Wave parameters such as significant wave height (H_s), peak wave period (T_p), and mean wave direction (T_m) extracted from the coupled Delft3D-SWAN simulations form the basis for calculating the wave energy flux (P) at the jetty location. The wave energy flux is computed using:

$$P = \rho g H_s^2 C^g$$

where ρ is the water density, g is gravitational acceleration, and Cg is the group velocity, derived from wave period and water depth.

4. Results and Discussion

4.1 Hydrodynamic Model Calibration and Validation

To assess the performance of the Delft3D-HD model, calibration was conducted using observational data from ADCP1, while ADCP2 served for independent validation, both instruments recorded continuous time series of tidal water levels and current velocities during a representative monitoring period that included both spring and neap tidal conditions. The calibration and validation were conducted with iterative adjustments to bottom friction (Manning's n = 0.02–0.03) and horizontal eddy viscosity (0.1–0.5 m²/s) until convergence was achieved. The calibration prioritized:

1. Tidal phase alignment (critical for flap submersion timing)
2. Current velocity profiles (for torque load estimation)
3. Directional consistency (to assess wave-current misalignment effects)

ADCP1 was positioned near the northeastern jetty region, where relatively stable tidal flows dominate. Calibration focused on fine-tuning model parameters such as bottom roughness, eddy viscosity, and boundary condition smoothing to best reproduce observed conditions. Validation was carried out using ADCP1 and ADCP2 to assess the model performance under different local hydrodynamic conditions. ADCP2 is located southwest of ADCP1, in a more hydrodynamically variable zone influenced by local bathymetric gradients and jetty-induced flow distortion. The comparison between measured and simulated results indicates that the model maintained good predictive capability for water level and current direction, while current-speed performance was more variable. Model performance was quantified using range-normalised RMSE and NSE (Table 3). The table has been reconstructed so that the metric basis and units are explicit: water-level and current-speed RMSE values are expressed as percentages of the observed range, current-direction RMSE is expressed in degrees, and NSE is dimensionless. The reconstructed validation statistics indicate good model skill for water level and current direction, while current-speed variability remains more difficult to reproduce because of phase shifts, slack-water sensitivity and local jetty-induced flow distortion.

Table 3. Validation statistics for ADCP stations, showing metric basis and units clearly (N = 12,288 samples).

Model output	Statistic / basis	Unit	ADCP1	ADCP2
Water level	Range-normalised RMSE	% of observed tidal range	9.83	9.57
Current speed	Range-normalised RMSE	% of observed current-speed range	19.67	19.51

Current direction	RMSE	degrees	19.58	19.58
Water level	NSE	dimensionless	0.85	0.82
Current speed	NSE	dimensionless	-0.17	-0.20
Current direction	NSE	dimensionless	0.95	0.96

The sub-10% water-level RMSE values indicate good reproduction of tidal elevations for feasibility-level hydrodynamic screening. In addition, the water-level NSE values of 0.85 and 0.82 for ADCP1 and ADCP2, respectively, indicate strong model skill in reproducing the observed tidal elevation pattern and temporal water-level variability at both stations.

For current direction, the model also demonstrates strong agreement with field observations. The directional RMSE values are approximately 19.58° at both ADCP stations, while the NSE values of 0.95 and 0.96 for ADCP1 and ADCP2, respectively, indicate that the model successfully captures the dominant current orientation and directional variability within the study area. These error levels are comparable to those reported in recent Southeast Asian coastal modelling studies (Ng et al., 2021).

For tidal current speed, the range-normalised RMSE values are approximately 19.7% and 19.5% for ADCP1 and ADCP2, respectively. These values suggest that the absolute prediction error remains within a reasonable range relative to the observed current-speed variation. However, the corresponding NSE values of -0.17 and -0.20 indicate limited model skill in reproducing the detailed temporal variability of current speed. This weaker NSE performance is likely influenced by the sensitivity of current-speed statistics to phase shifts, peak-current timing, slack-water periods, and localised hydrodynamic effects associated with jetty-induced flow distortion and bathymetric gradients.

Overall, the validation results show that the Delft3D-HD model is well calibrated for tidal water level and current direction, while the current-speed predictions are acceptable in terms of range-normalised RMSE but should be interpreted with caution based on NSE. Despite the lower NSE values for current speed, the model provides a robust hydrodynamic foundation for subsequent wave coupling and wave-energy potential assessments in the Bintulu coastal area.

A. Implications for Hinged-Flap WECs

For energy prediction, accurate tidal phases (<10% RMSE) ensure reliable prediction of flap operational windows (Whittaker & Folley, 2012; IEC, 2019). The current velocity errors <20% introduce <5% uncertainty in monsoon-induced load estimates (Zhang et al., 2022). Structurally, directional RMSE <20° enables proper assessment of the wave-current misalignment on hinge fatigue (IEC, 2019) and scour potential from oblique currents (Whitehouse, 2018).

B. Coupling of HD and Wave Model

The Delft3D-HD model was calibrated using two ADCP datasets collected near the Bintulu jetty. Simulated tidal elevations and current velocities showed strong agreement with observations, with root mean square error (RMSE) values of less than 10% for water levels and less than 20% for current speed, as shown in Figure 7a and Figure 7b.

The coupled Delft3D-WAVE and SWAN models captured the transformation of incident wave energy across the domain. Wave shoaling and directional spreading effects were particularly evident near the jetty head and leeward side, validating the importance of high-resolution nearshore modelling.

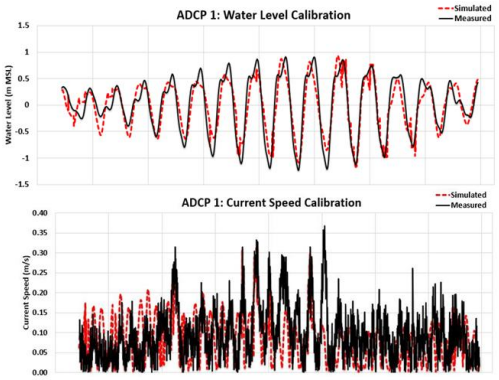

Fig. 7a-Model calibration for tidal level and current speed at ADCP 1

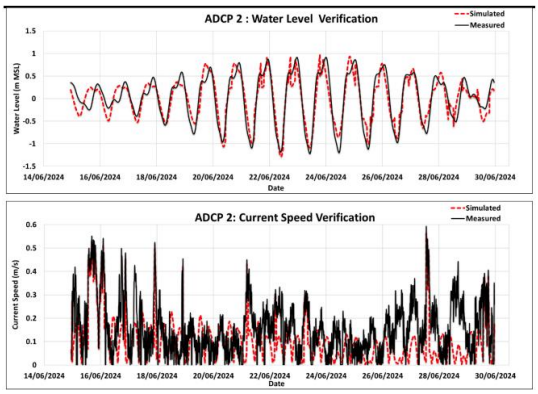

Fig.7b-Model validation for tidal level and current speed at ADCP 2

The coupled simulations over a representative year revealed that average significant wave heights (H_s) ranged from 0.8–1.2 m, with dominant peak periods (T_p) between 6–8 s. The wave height covering typical NE and SW are given in Figure 8a and 8b. Peak wave conditions during northeast monsoon

and southwest events exceeded 1.5 m in H_s (Figure 8c and 8d).

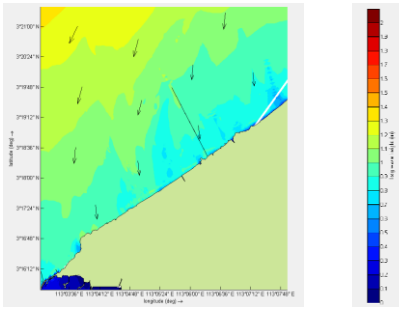

Fig.8a-Typical wind-generated wave field from the NE direction

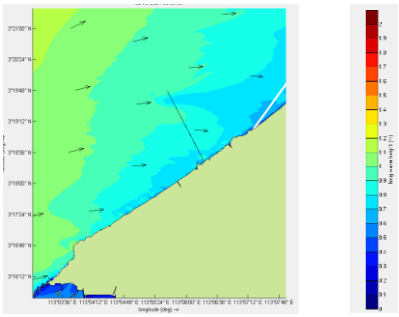

Fig. 8b-Typical wind-generated wave field from the SW direction

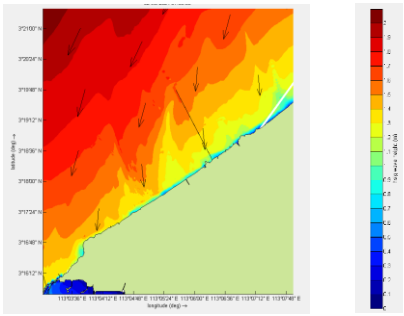

Fig.8c-Peak wind-generated wave field from the NE direction

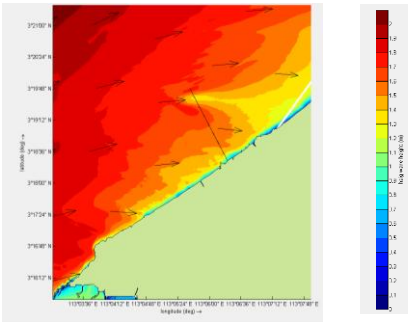

Fig.8d-Peak wind-generated wave field from the SW direction

D. Wave Energy Flux Estimation

Wave power flux (P) is the rate at which wave energy passes through a unit width of wave front (usually expressed in kW per meter). It represents the energy available from ocean waves that can potentially be harnessed by wave energy converters.

The study considered two primary seasonal regimes:

- Northeast Monsoon (NE): Prevailing wave direction from the northeast, with modelled significant wave heights (H_s) of 1-1.2 m and peak wave periods (T_p) of 7–8 s.
- Southwest Monsoon (SW): Sheltered wave exposure, with Hs typically between 0.8–1.2 m and T_p around 6–8 s.

Wave energy flux per unit wave crest length (P) was computed using the standard deep-water wave power approximation reported by Falnes (2007):

$$P = \frac{\rho g^2}{64\pi} H_s^2 T_p$$

where ρ = 1025 kg/m³ is seawater density, g = 9.81 m/s² is gravitational acceleration, Hs is significant wave height and Tp is peak wave period.

Substituting typical NE monsoon values, the estimated wave energy flux reaches approximately 3.4–5.6 kW/m. In contrast, SW monsoon conditions yield a much lower flux of 1.9–5.6 kW/m, reflecting limited wave energy potential during this season.

Despite the modest energy levels, the consistency and directionality of NE monsoon waves make the site suitable for hinged-type Wave Energy Converters (WECs). These devices are designed to capture energy from oscillatory pitching motion induced by incoming waves. When strategically oriented perpendicular to predominant NE wave directions, hinged-type WECs can operate effectively under such moderate conditions.

Device-level energy output was therefore estimated using the scenario-based AEP method in Sections E to H rather than relying only on theoretical wave flux. This ensures that the reported results quantify extractable energy after applying practical WEC performance and operational factors.

These findings support the feasibility of hinged-type WEC deployment along the northeast-facing jetty segment, where directional wave approach and available energy flux are most favourable. The use of high-resolution, coupled Delft3D-SWAN simulations ensures that wave dynamics and seasonal variability are accurately captured for technology planning and optimisation.

E. Hinged-Flap WECs Performance and Energy Output

The wave energy resource assessed through the coupled Delft3D-HD and SWAN modelling system was used to evaluate the potential performance of hinged-flap Wave Energy Converters (WECs) deployed nearshore along the Bintulu jetty. These WECs operate on the principle of converting the pitching motion of a seabed-mounted flap, hinged at the base, into usable mechanical or electrical energy. They are particularly suited for moderate-energy wave climates with dominant unidirectional wave forcing (Whittaker and Folley, 2012).

F. Device Configuration and Site Conditions

The preferred deployment configuration consists of flap-type WECs aligned perpendicular to the dominant Northeast Monsoon and Southwest wave direction, where significant wave heights range from 0.8 to 1.2 m and wave periods from 6 to 8 seconds, as derived from SWAN model outputs. These sea states fall within the optimal operating range of commercially developed hinged-flap devices, which typically activate above a threshold wave height of 0.25 m (Folley et al., 2007).

Hydrodynamic interaction simulations were carried out using device response curves adapted from benchmark bottom-hinged flap designs, including the Oyster WEC. The response curves were applied to the SWAN spectral outputs to estimate absorbed power as a function of wave frequency, spectral energy density and flap response. This frequency-domain representation follows established WEC assessment practice for early-stage feasibility studies (Falnes, 2007; Whittaker and Folley, 2012; Pecher and Kofoed, 2017).

G. Power Performance

Following the frequency-domain WEC response-function approach reported by Falnes (2007), Whittaker and Folley (2012), and Pecher and Kofoed (2017), the time-averaged absorbed power per unit was estimated as:

$$P_{avg} = \int_0^\infty R\,(\omega) S(\omega) d\omega$$

Where

R(ω) is the frequency-dependent response function of the hinged-flap device, representing the combined effects of flap geometry, hinge stiffness and PTO damping.
S(ω) is the wave spectral energy density obtained from the SWAN model at the proposed deployment location.

H. Annual Energy Production

The performance of hinged-type Wave Energy Converters (WECs) along the Bintulu coastline was evaluated based on wave climate data simulated using the Delft3D-SWAN model. The spectral wave simulations captured the site-specific wave energy conditions, particularly during the Northeast Monsoon (November to March), when wave activity is most pronounced. During this period, the significant wave height ranges from 1.0 to 1.2 m, with peak wave periods of 7 to 8 seconds, resulting in a calculated wave energy flux of approximately 3.4 to 5.6 kW/m along the jetty-facing coastline.

To estimate the realistic energy output of a hinged-type wave energy converter (WEC) array along the Bintulu jetty, a performance-based energy production model was developed using SWAN-derived wave climate data, technical conversion efficiencies, and operational constraints. Hinged-flap WECs, which operate by converting the oscillatory pitching motion of waves into mechanical or electrical energy, are well-suited to such conditions (Folley, Whittaker and Henry, 2007; Whittaker and Folley, 2012). For this feasibility-level assessment, device spacing of 30 to 50 m was adopted as a preliminary array-layout assumption to allow a relatively high-density installation along the coastline while limiting near-field hydrodynamic interaction between adjacent flap units.

The accuracy of the power-performance prediction is therefore interpreted at feasibility level. The hydrodynamic model reproduces water-level and current-direction variability well, but current-speed NSE is lower; hence the energy output is reported as a conservative-to-optimistic range rather than a single deterministic value. The dominant uncertainties are the selected CWR, PTO efficiency, annual availability, array interaction loss and the absence of device-specific field power-curve validation. A pilot-scale deployment with measured WEC output is recommended before detailed investment or final design. While previous estimates considered theoretical wave energy flux alone, practical deployment requires accounting for device-specific factors such as capture width ratio (CWR), power take-off (PTO) efficiency, annual availability, and array interaction losses (Falnes, 2007; Pecher and Kofoed, 2017).

Based on SWAN model simulations, the Northeast Monsoon season provides the most energetic sea states, with significant wave heights (Hs) ranging from 1.0 to 1.2 m and peak wave periods (Tp) of 7 to 8 s. The corresponding deep water wave power flux (P) is estimated between 3.4 and 5.6 kW/m, using standard deep water wave energy formulas (Falnes, 2007).

For a 3 km deployment of hinged-flap WECs, the following assumptions are used:

Table 4. Assumptions used for hinged-flap WEC annual energy production estimation.

Parameter	Value Range	Reference
Deployment length	3,000 m	Site assumption
Device spacing	30–50 m	This study; preliminary feasibility assumption
Number of WEC units (N)	60–100	Derived
Capture Width Ratio (CWR)	20–35%	This study; feasibility-level assumption
PTO efficiency (η_{pto})	80–90%	Pecher and Kofoed (2017)
Availability (A)	85–95%	OES, 2023
Array interaction loss (L_array)	5–15%	Babarit (2013)

The average absorbed power per unit was then simplified into a capture-width formulation for array-scale energy estimation, consistent with early-stage WEC performance assessments (Falnes, 2007; Pecher and Kofoed, 2017):

$$P_{avg} = P_{wave} \times CWR$$

Annual Energy Production (AEP) was calculated by applying PTO efficiency, availability and array-interaction losses to the absorbed power, following the engineering assumptions summarised in Table 4 (Babarit, 2013; OES, 2023):

$AEP_{unit} = P_{avg} \times \eta_{PTO} \times A \times (1 - L_{array}) \times 8760$

I. Scaled Annual Output

For the mid-point scenario, an average wave power of Pwave = 3.94 kW/m was adopted from the NE and SW seasonal range. The following mid-point parameters were used for comparison with the conservative and optimistic scenarios:

- Capture Width Ratio (CWR) = 0.275 (27.5%)
- Power take-off efficiency (ηPTO) = 0.85
- Availability (A) = 0.90
- Array interaction loss (Larray) = 0.10
- Number of WEC units (N) = 80, based on a 3 km deployment length with approximately 37.5 m spacing.

In the conservative scenario, using a site wave power of 2.66 kW/m, a capture width ratio (CWR) of 0.20, PTO efficiency of 80%, availability of 85%, and array interaction loss of 15%, the annual energy production (AEP) per unit is estimated at approximately 2.69 MWh/year. For a farm with between 60 and 100 devices, this translates to a total AEP in the range of 161 to 269 MWh/year. This represents a conservative, technically grounded estimate.

If higher CWR or longer device operational hours are achieved, total AEP could exceed 1,000 MWh/year, making this deployment scale suitable for powering coastal infrastructure or supporting microgrids. In the optimistic scenario, using a site wave power of 5.65 kW/m, a CWR of 0.35, PTO efficiency of 90%, availability of 95%, and array interaction loss of 5%, the AEP per unit is estimated at approximately 14.06 MWh/year. For a farm of 60 to 100 devices, this corresponds to a total AEP in the range of 844 to 1,406 MWh/year.

Table 5. Summary of scaled annual WEC output scenarios for the proposed 3 km Bintulu jetty deployment.

Note: household estimates assume 4,000 kWh/year per household and exclude grid/storage losses; values are intended for feasibility screening and should be updated using measured device power curves during pilot testing.

Scenario	Key assumptions	AEP per unit (MWh/year)	Farm AEP (MWh/year)	Approx. households/year
Conservative	Pwave = 2.66 kW/m; CWR = 0.20; PTO = 0.80; A = 0.85; Larray = 0.15; N = 60-100	2.69	161-269	40-67
Mid-point	Pwave = 3.94 kW/m; CWR = 0.275; PTO = 0.85; A = 0.90; Larray = 0.10; N = 80	6.54	523	131
Optimistic	Pwave = 5.65 kW/m; CWR = 0.35; PTO = 0.90; A = 0.95; Larray = 0.05; N = 60-100	14.06	844-1,406	211-352

This seasonal variability emphasises the importance of deploying WEC systems optimised for monsoonal climates, where energy yield is concentrated within specific windows of the year. Nonetheless, the integration of hinged-flap WECs along existing jetty infrastructure offers a promising approach to nearshore wave energy extraction, with significant potential for hybridisation with solar or storage systems for continuous power supply.

In the context of Malaysia, average annual electricity consumption per household ranges between 3,500 and 4,500 kWh/year, depending on urbanisation, appliance ownership, and income level (TNB, 2022). Using a national average of 4,000 kWh/year as a representative value, the number of households supported by the wave energy system is calculated as:

Households supplied = AEP (kWh/year) / 4,000

Assuming the average Malaysian household consumes about 4,000 kWh of electricity per year and ignoring grid/storage losses, the conservative scenario—with a total annual energy production (AEP) of 161–269 MWh/year for the entire wave energy farm could supply electricity to approximately 40–67 households per year, calculated by dividing the farm's AEP range by the per-household annual demand.

In the optimistic scenario with an AEP of 844–1,406 MWh/year the farm could supply approximately 211–352 households per year, using the same calculation method. These values represent the theoretical maximum number of households powered annually under the given assumptions, without accounting for real-world efficiency losses in transmission or storage.

These figures indicate that the 3 km WEC array could potentially supply clean, renewable energy to approximately 40-352 households annually across the conservative-to-optimistic scenario range. The result directly translates the available wave resource into extractable energy output and household-equivalent supply, while recognising that final

Published by JPS Publishing
https://journal.water.gov.my

values depend on device selection, deployment density, PTO performance, array spacing and operational availability.

Moreover, because the wave energy yield aligns with the Northeast Monsoon season—when solar generation is reduced due to cloud cover—this system offers a complementary renewable supply that could improve grid resilience and reduce seasonal energy gaps.

Conclusion

A coupled Delft3D-HD and SWAN modelling framework was applied to assess the feasibility of deploying hinged-flap Wave Energy Converters (WECs) along 3 km of the Bintulu jetty. The amended analysis now links the wave resource to extractable energy using a transparent WEC performance formulation, supported by RMSE/NSE model validation and scenario-based AEP estimates. SWAN simulations identified the Northeast Monsoon as the primary operational window, with H_s of 1.0-1.2 m and T_p of 7-8 s, yielding 3.4-5.6 kW/m wave energy flux. After applying CWR, PTO efficiency, availability and array-loss assumptions, the estimated farm-scale AEP ranges from 161-269 MWh/year in the conservative case to 844-1,406 MWh/year in the optimistic case, equivalent to approximately 40-67 and 211-352 households, respectively. Overall, the results indicate that hinged-flap WEC deployment at the Bintulu jetty is technically feasible as a small-scale complementary renewable-energy option, particularly during monsoonal periods when wave energy is more consistent. However, because power prediction remains feasibility-level, pilot-scale testing, device-specific power-curve calibration, techno-economic optimisation and long-term metocean validation are recommended before full-scale implementation.

References

[1] Abdullah, W.N.A.W., Ismail, A., Hassan, M.R. & Karim, M.F. 2022. Sediment transport dynamics and seabed morphology in the South China Sea shelf off Sarawak. *Marine Geology*, 443: 106710.

[2] Babarit, A. 2013. On the park effect in arrays of oscillating wave energy converters. *Renewable Energy*, 58, pp.68–78.

[3] Deltares. 2023. *Delft3D-FLOW, SWAN and Delft Dashboard User Manuals*. Version 4.03. Delft: Deltares.

[4] Egbert, G.D. & Erofeeva, S.Y. 2002. Efficient inverse modeling of barotropic ocean tides. *Journal of Atmospheric and Oceanic Technology*, 19(2), pp.183–204.

[5] Falnes, J. 2007. A review of wave-energy extraction. *Marine Structures*, 20(4), pp.185–201.

[6] Folley, M., Whittaker, T. & Henry, A. 2007. The effect of water depth on the performance of a small surging wave energy converter. Ocean Engineering, 34(8–9), pp.1265–1274.

[7] GROW (Global Reanalysis of Ocean Waves). 2012. *Global Reanalysis of Ocean Waves 2012 Dataset*. Japan Meteorological Agency and Japan Oceanographic Data Center. Available at: https://www.jodc.go.jp [Accessed 21 Jun. 2025].

[8] IEC. 2019. *IEC TS 62600-2: Wave energy converter design requirements*. Geneva: International Electrotechnical Commission.

[9] Mazlan, M.S., Idris, N.S., Rahman, M.R. & Lim, W.L. 2020. Seasonal variation of wave climate in Malaysian waters. *Journal of Ocean and Coastal Engineering*, 17(2), pp.101–112.

[10] Moriasi, D.N., Arnold, J.G., Van Liew, M.W., Bingner, R.L., Harmel, R.D. & Veith, T.L. 2007. Model evaluation guidelines for systematic quantification of accuracy in watershed simulations. Transactions of the ASABE, 50(3), pp.885-900.

[11] Ng, C.K., Tan, L.P. & Wong, P.P. 2021. Hydrodynamic modelling of monsoonal currents in Southeast Asia. *Journal of Coastal Research*, 37(2), pp.312–325.

[12] OES (Ocean Energy Systems). 2023. *Annual Report 2022*. International Energy Agency Technology Collaboration Programme on Ocean Energy Systems.

[13] Omar, H. & Samad, M.A. 2023. Coastal infrastructure integration for wave energy development in Southeast Asia. *Renewable Energy Advances*, 12(1), pp.45–58.

[14] Pecher, A. & Kofoed, J.P. (eds.) 2017. Handbook of Ocean Wave Energy. Cham: Springer.

[15] Tan, S.H., Lim, C.H. & Wong, P.L. 2021. Sediment characteristics and depositional environments off the coast of Borneo. *Journal of Asian Earth Sciences*, 213: 104812.

[16] TNB (Tenaga Nasional Berhad). 2022. *Electricity Consumption Data*. [online] Available at: https://www.tnb.com.my [Accessed 21 Jun. 2025].

[17] Weatherall, P., Marks, K.M., Jakobsson, M., Schmitt, T., Tani, S., Arndt, J.E., Rovere, M., Chayes, D., Ferrini, V., Wigley, R. & Anderson, C. 2015. A new digital bathymetric model of the world's oceans. *Earth and Space Science*, 2(8), pp.331–345.

[18] Whitehouse, R.J.S. 2018. *Scour in Marine Environments*. London: ICE Publishing.

[19] Whittaker, T. & Folley, M. 2012. Nearshore oscillating wave surge converters and the development of Oyster. *Philosophical Transactions of the Royal Society A: Mathematical, Physical and Engineering Sciences*, 370(1959), pp.345–364.

[20] Yusof, M.N., Zainal, M.Z., Abdullah, M.F. & Ismail, S. 2019. Geotechnical assessment of offshore pile foundations in the South China Sea. *Geotechnical Engineering Journal of the SEAGS & AGSSEA*, 50(4), pp.62–70.

[21] Zhang, D., Li, W. & Lin, Y. 2022. Load uncertainty in tropical monsoon wave climates. *Applied Ocean Research*, 118: 102972.